Control Aspects for Energy-Efficient and Sensorless AC Motor Drives

Zengcai Qu

Aalto University

DOCTORAL DISSERTATIONS

Aalto University publication series
DOCTORAL DISSERTATIONS 85/2015

Control Aspects for Energy-Efficient and Sensorless AC Motor Drives

Zengcai Qu

A doctoral dissertation completed for the degree of Doctor of Science (Technology) to be defended, with the permission of the Aalto University School of Electrical Engineering, at a public examination held at the lecture hall S3 of the school on 10 July 2015 at 12.

Aalto University
School of Electrical Engineering
Department of Electrical Engineering and Automation
Industrial Electronics and Electric Drives

Supervising professors
Prof. Jorma Luomi
Prof. Marko Hinkkanen

Thesis advisor
Prof. Marko Hinkkanen

Preliminary examiners
Prof. Radu Iustin Bojoi, Politecnico di Torino, Italy
Prof. Oskar Wallmark, KTH Royal Institute of Technology, Sweden

Opponent
Prof. Giacomo Scelba, University of Catania, Italy

Aalto University publication series
DOCTORAL DISSERTATIONS 85/2015

ISBN 978-952-60-6252-5 (printed)
ISBN 978-952-60-6253-2 (pdf)
ISSN-L 1799-4934
ISSN 1799-4934 (printed)
ISSN 1799-4942 (pdf)
http://urn.fi/URN:ISBN:978-952-60-6253-2

Unigrafia Oy
Helsinki 2015

Finland

441 697
Printed matter

Author
Zengcai Qu

Name of the doctoral dissertation
Control Aspects for Energy-Efficient and Sensorless AC Motor Drives

Publisher School of Electrical Engineering

Unit Department of Electrical Engineering and Automation

Series Aalto University publication series DOCTORAL DISSERTATIONS 85/2015

Field of research Industrial Electronics and Electric Drives

Manuscript submitted 23 February 2015 **Date of the defence** 10 July 2015

Permission to publish granted (date) 8 May 2015 **Language** English

☐ **Monograph** ☒ **Article dissertation (summary + original articles)**

Abstract

This research proposes control methods for improving the energy efficiency and stability of sensorless AC motor drives. The study focuses on induction motors (IMs) and synchronous reluctance motors (SyRMs). Loss-minimizing methods are developed for both IM and SyRM drives. The loss-minimizing control applies dynamic space-vector motor models which take into account hysteresis losses and eddy-current losses as well as the magnetic saturation. The minimum points of the loss function are numerically searched in order to calculate the efficiency-optimal control variable. Magnetic saturation effects can affect the energy optimization more significantly than core-loss parameters. Additionally, flux-angle and rotor-angle estimation methods in sensorless drives are also sensitive to inductance parameters. A saturation model was proposed for SyRMs using explicit power functions. The proposed model takes into account cross saturation and fulfills the reciprocity condition. In order to improve the stability of the sensorless IM drives, especially at low speeds, a gain scheduling method was proposed for a full-order flux observer. The observer gains are selected as functions of the rotor speed estimate in order to improve the damping and robustness of the closed-loop system. The observer is augmented with a stator-resistance adaptation scheme in the low-speed region. In high-speed applications with limited sampling frequency, dynamic performance of the discrete-time approximation of a continuous-time controller can dramatically decrease, and can, in the worst case, even become unstable. A discrete-time current controller was proposed for SyRMs. The current controller is designed based on the exact discrete-time motor model that includes the effects of the zero-order hold and delays. The dynamic performance and robustness are improved, especially at low sampling to fundamental frequency ratios.

Keywords discrete-time control, energy efficiency, induction motor, magnetic saturation, observer, speed sensorless, stability, synchronous reluctance motor

ISBN (printed) 978-952-60-6252-5 **ISBN (pdf)** 978-952-60-6253-2

ISSN-L 1799-4934 **ISSN (printed)** 1799-4934 **ISSN (pdf)** 1799-4942

Location of publisher Helsinki **Location of printing** Helsinki **Year** 2015

Pages 121 **urn** http://urn.fi/URN:ISBN:978-952-60-6253-2

Preface

The research work was carried out at the Department of Electrical Engineering and Automation, Aalto University. Part of my research is funded by the Academy of Finland.

Most of all, I would like to thank my professor Marko Hinkkanen who has strongly supported my work and provided me with most of the support and instruction in my research and publication writing. I could not have completed this work done without his guidance and help. I would also like to remember my professor Jorma Luomi who passed away in December 2011. He was a good leader and a distinguished scholar. He supported my work from the very beginning of my project until his very last days. Professor Lennart Harnefors from ABB Sweden has closely cooperated with our research group and he offered good comments and helped with one of my publications. I would also like to express my gratitude to Prof. Jorma Kyyrä for the interesting courses in power electronics and Prof. Antero Arkkio for the helpful lectures in electromechanics.

I want to thank all my colleagues—Mikaela Ranta, Toni Tuovinen, Matti Liukkonen, Seppo Saarakkala, Jarno Kukkola, Jussi Koppinen and Asad Awan—for the good working atmosphere and warm, pleasant, friendly, and relaxed relationships. We shared opinions not only about the problems in our research work but also the happiness, pressure and stories in life. I want to thank Antti Piippo from ABB and Janne Salomäki from Konecranes for the discussions during meetings and dinners. Ranran Lin, who was earlier in the Electromechanics group and now working at ABB Shanghai provided me considerable help in studies and life. I cannot list all the names of my friends, whom I met during the last six years in Finland, it is because of them that my life became more interesting and joyful.

Finally, I would also like to thank my wife Xiuwen Cai and my little son Juho Qu for the happiness they have brought to my life. You light up my

life and make me enjoy the warmth of the family. My sweet family makes me feel at home no matter where we are. I would also thank my parents who had supported me with their arduous labor and endless love.

Espoo, May 22, 2015,

Zengcai Qu

Contents

List of Publications

This thesis consists of an overview and of the following publications which are referred to in the text by their Roman numerals.

I Z. Qu, M. Ranta, M. Hinkkanen, and J. Luomi. Loss-minimizing flux level control of induction motor drives. *IEEE Transactions on Industry Applications*, vol. 48, issue 3, pp. 952-961, May-June 2012.

II Z. Qu, T. Tuovinen, and M. Hinkkanen. Inclusion of magnetic saturation in dynamic models of synchronous reluctance motors. In *Proc. XXth International Conference on Electrical Machines (ICEM 2012)*, Marseille, France, Sep. 2012.

III Z. Qu and M. Hinkkanen. Loss-minimizing control of synchronous reluctance motors — a review. In *Proc. IEEE International Conference on Industrial Technology (ICIT 2013)*, Captown, South Africa, Feb. 2013.

IV Z. Qu, T. Tuovinen, and M. Hinkkanen. Minimizing losses of a synchronous reluctance motor drive taking into account core losses and magnetic saturation. In *the 16th Conference on Power Electronics and Applications, EPE'14-ECCE Europe*, Lappeenranta, Finland, Aug. 2014.

V Z. Qu, M. Hinkkanen, and L. Harnefors. Gain scheduling of a full-order observer for sensorless induction motor drives. *IEEE Transactions on Industry Applications*, vol. 50, issue. 6, pp. 3834-3845, Nov.-Dec. 2014.

VI M. Hinkkanen, Z. Qu, H. A. A. Awan, T. Tuovinen, and F. Briz. Current control for IPMSM drives: direct discrete-time pole-placement

design. In *IEEE Workshop on Electrical Machines Design Control and Diagnosis (WEMDCD)*, Turin, Italy, Mar. 2015.

Author's Contribution

Publication I: "Loss-minimizing flux level control of induction motor drives"

The author wrote the paper under the guidance of Prof. Luomi and Prof. Hinkkanen. Dr. Ranta performed the parameter sensitivity analysis and participated in the writing of the publication.

Publication II: "Inclusion of magnetic saturation in dynamic models of synchronous reluctance motors"

The author wrote the paper under the guidance of Prof. Hinkkanen. Dr. Tuovinen performed the measurements and participated in the writing of the paper.

Publication III: "Loss-minimizing control of synchronous reluctance motors — a review"

The author wrote the paper under the guidance of Prof. Hinkkanen.

Publication IV: "Minimizing losses of a synchronous reluctance motor drive taking into account core losses and magnetic saturation"

The author wrote the paper under the guidance of Prof. Hinkkanen. Dr. Tuovinen contributed by commenting on the manuscript.

Publication V: "Gain scheduling of a full-order observer for sensorless induction motor drives"

The author wrote the paper under the guidance of Prof. Hinkkanen. Prof. Harnefors gave comments on the manuscript.

Publication VI: "Current control for IPMSM drives: direct discrete-time pole-placement design"

The author was responsible for the robustness analysis against parameter errors and the experiments. The author also participated in the writing of the paper.

Symbols and Abbreviations

Symbols

G_{Ft}	Eddy-current loss factor
i_{a}, i_{b}, i_{c}	Phase current
$i_{\mathrm{d}}, i_{\mathrm{q}}$	Direct-axis and quadrature-axis currents
$i_{\mathrm{md}}, i_{\mathrm{mq}}$	Direct-axis and quadrature-axis magnetizing currents
$\boldsymbol{i}_{\mathrm{r}}$	Rotor current of T model
$\boldsymbol{i}_{\mathrm{R}}$	Rotor current of inverse-Γ model
$\boldsymbol{i}'_{\mathrm{R}}$	Rotor current of Γ model
$\boldsymbol{i}_{\mathrm{s}}$	Stator current in synchronous coordinates
$\boldsymbol{i}_{\mathrm{s}}^{\mathrm{s}}$	Stator current in stator coordinates
$i_{\mathrm{s}\alpha}$, $i_{\mathrm{s}\beta}$	Stator-current components in stator coordinates
$i_{\mathrm{sd}}, i_{\mathrm{sq}}$	Stator-current components in synchronous coordinates
$\boldsymbol{I}$	Identity matrix
$\boldsymbol{J}$	Orthogonal rotation matrix
$L_{\mathrm{d}}, L_{\mathrm{q}}$	Direct-axis and quadrature-axis inductances
L_{du}	Unsaturated direct-axis inductance
$\boldsymbol{L}$	Inductance matrix
L_{M}	Magnetizing inductance of inverse-Γ model
L'_{M}	Magnetizing inductance of Γ model
L_{σ}	Leakage inductance of inverse-Γ model
L'_{σ}	Leakage inductance of Γ model
P_{Cu}	Copper losses
P_{Ft}	Eddy-current losses
P_{Hy}	Hysteresis losses

P_{loss}	Total of copper losses and core losses
R_{c}	Core-loss resistance
R_{r}	Rotor resistance
R_{R}	Rotor resistance of inverse-Γ model
R'_{R}	Rotor resistance of Γ model
R_{s}	Stator resistance
T_{e}	Electromagnetic torque
$\boldsymbol{u}_{\mathrm{s}}$	Stator voltage
α	Magnetic saturation model parameter
α_{c}	Current control bandwidth
β	Magnetic saturation model parameter
θ	Angle of reference frame
Λ_{Hy}	Hysteresis loss factor
$\psi_{\mathrm{d}}, \psi_{\mathrm{q}}$	Direct-axis and quadrature-axis stator-flux components
$\boldsymbol{\psi}_{\mathrm{R}}$	Rotor flux linkage of inverse-Γ model
$\boldsymbol{\psi}'_{\mathrm{R}}$	Rotor flux linkage of Γ model
$\boldsymbol{\psi}_{\mathrm{s}}$	Stator flux linkage
ω_{m}	Electrical angular speed of rotor
ω_{s}	Stator angular frequency

Abbreviations

AC	Alternative current
DC	Directive current
DTC	Direct torque control
IGBT	Insulated-gate bipolar transistor
IM	Induction motor
PWM	Pulse-width modulation
SyRM	Synchronous reluctance motor
ZOH	Zero-order hold

1. Introduction

Three-phase AC motors provide a large amount of the mechanical power used in modern industry. Induction motors (IMs) are favored due to their simplicity, ruggedness, low cost, and ability to self-start simply by direct connection to the mains. Synchronous reluctance motors (SyRMs) have become increasingly important alternatives to IMs. In addition to their simple and robust structure, the absence of the rotor winding has resulted in higher efficiency than that achievable with IMs.

Typical electric drive applications include compressed air, pumping and fan systems, which account for the highest industrial electricity consumption. Adjusting the motor speed can result in a significant power loss reduction. Nowadays, an increasing number of electrical machines are fed by frequency converters to save energy. The frequency converter transforms the standard three-phase line voltage into a variable-frequency and variable-voltage output to control the motor. It typically consists of a rectifier, a DC link and a pulse-width modulated (PWM) inverter.

In 1958, the first thyristor, which was called a silicon-controlled rectifier, was commercially introduced by General Electric (Gutzwiller, 1960). The introduction of thyristors brought about the era of power electronics. In the 1960s and 1970s, the technologies of power electronics based on the thyristor underwent rapid development. Research on variable speed AC drives was boosted by the introduction of new power semiconductor devices and advanced converter topologies. Today, IGBTs are commonly used in the frequency converters, and wide bandgap power semiconductor devices are expected to become the new generation of power devices (Millan et al., 2014).

The speed of an IM can be controlled by varying the frequency of the power supply. However, in order to maintain a constant flux magnitude, the applied voltage must also be changed in the same proportion as the

frequency. This speed control method is known as Volts per Hertz or V/f control (Schönung and Stemmler, 1964). However, V/f control is based on steady-state characteristics, and its dynamic performance at the transient state is far from ideal.

Vector control, also called field-oriented control, was developed by Blaschke (1972). Vector control is commonly used in variable speed drives. The three-phase stator currents are transformed to two orthogonal components which decouple the torque-producing current and the flux-producing current. This enables AC motors to be controlled as simply as DC motors. Direct torque control (DTC) was proposed by Takahashi and Noguchi (1986) and Depenbrock (1988), which is based on hysteresis control of both flux and torque using an optimum PWM output voltage. DTC employs a switching table for selecting the optimum inverter output voltage vectors, thus enabling a fast torque response.

Apart from variable speed drives, loss-minimizing methods have also been used to further increase the energy efficiency of electrical machines. For any given torque and speed, the total losses in an electrical machine depend on the flux level. Generally, loss-minimizing controllers can be divided into two categories (Vukosavic and Levi, 2003; Bazzi and Krein, 2010): the *loss-model based controller*, which uses the motor model and parameters to calculate the loss-minimizing currents (Tsivitse and Klingshirn, 1971), and the *online search controller*, which adjusts the current vector online based on the feedback from input power measurements (Kirschen et al., 1985). This dissertation focuses on model-based methods. The losses are modeled as a function of motor parameters and operating points. The conditions for loss minimization can be determined by searching the minimum of the loss function with respect to the control variable.

Electric drives without a speed or position sensor represent advantages in terms of low costs, simplicity and high reliability. The flux estimate is extracted from measured voltages and currents at the terminals. Various flux estimators, including open-loop estimators and closed-loop observers, have been proposed over the last two decades. These methods differ with respect to their stability, accuracy, and parameter sensitivity. Flux estimators based on the standard dynamic motor model are known to be sensitive to parameter errors in the lowest speed region (Harnefors and Hinkkanen, 2014). In order to improve the stability at low speeds, the gains of a closed-loop flux observer should be properly selected.

The main aim of this dissertation is to develop control methods for loss-

minimizing and speed-sensorless IM and SyRM drives. The proposed controllers improve the energy efficiency, stability, and dynamic performance of AC motor drives. The research includes the following subtopics:

- Loss-minimizing controllers are proposed for both IMs and SyRMs that reduce steady-state losses in the motors.
- Magnetic saturation effects of SyRMs are modeled using explicit functions which can take into account cross saturation and the reciprocity condition.
- A gain-scheduling design of a full-order flux observer for sensorless IM drives is proposed to improve the robustness against model parameter errors at the lowest speeds.
- In order to improve the performance and stability of SyRMs, especially when the ratio of the sampling frequency to the fundamental frequency is low, a discrete current controller is designed based on the exact discrete SyRM model.

The following chapters of this dissertation are organized as follows: Chapter 2 introduces the space-vector dynamic models of the IM and the SyRM, as well as the magnetic saturation model for SyRMs. Chapter 3 describes the loss-minimizing methods. Chapter 4 presents the flux observer design for speed-sensorless IM control. Chapter 5 introduces an exact discrete-time model for the SyRM and a current controller design in the discrete-time domain. Chapter 6 summaries the publications and lists the abstracts and contributions of each publication. Finally, Chapter 7 offers the conclusions drawn from this work. The publications included in this dissertation are reprinted at the end.

2. System Models

2.1 Space Vectors

A symmetric three-phase system can be described as an equivalent two-phase system. For example, the three-phase stator currents in an electrical machine can be transformed into a real-valued space vector:

$$\boldsymbol{i}_{\mathrm{s}}^{\mathrm{s}} = \begin{bmatrix} i_{\mathrm{s}\alpha} \\ i_{\mathrm{s}\beta} \end{bmatrix} = \begin{bmatrix} \frac{2}{3} & -\frac{1}{3} & -\frac{1}{3} \\ 0 & \frac{1}{\sqrt{3}} & -\frac{1}{\sqrt{3}} \end{bmatrix} \begin{bmatrix} i_{\mathrm{a}} \\ i_{\mathrm{b}} \\ i_{\mathrm{c}} \end{bmatrix} \tag{2.1}$$

where i_{a}, i_{b} and i_{c} are the three-phase stator currents, and $i_{\mathrm{s}\alpha}$ and $i_{\mathrm{s}\beta}$ represent the orthogonal components of the real-valued space vector. The space vectors of other motor quantities can be defined in the same manner as the stator currents. In this thesis, vectors and matrices are denoted by boldface letters. Space vectors in stator coordinates are marked with the superscript s and their orthogonal components are denoted with the subscripts α and β.

The transformation from the stator coordinate system to the synchronous coordinate system, rotating at the synchronous speed ω_{s}, is given by

$$\boldsymbol{i}_{\mathrm{s}} = \begin{bmatrix} i_{\mathrm{sd}} \\ i_{\mathrm{sq}} \end{bmatrix} = \mathrm{e}^{-\boldsymbol{J}\theta} \boldsymbol{i}_{\mathrm{s}}^{\mathrm{s}} = \begin{bmatrix} \cos\theta & \sin\theta \\ -\sin\theta & \cos\theta \end{bmatrix} \begin{bmatrix} i_{\mathrm{s}\alpha} \\ i_{\mathrm{s}\beta} \end{bmatrix} \tag{2.2}$$

where $\theta = \int \omega_{\mathrm{s}} \mathrm{d}t$ is the angle between stator coordinates and synchronous coordinates. The orthogonal rotation matrix is $\boldsymbol{J} = \left[\begin{smallmatrix} 0 & -1 \\ 1 & 0 \end{smallmatrix}\right]$. The subscripts d and q refer to the synchronous reference frame. Space vectors in the synchronous reference frame are denoted without superscript.

2.2 Motor Models

2.2.1 IM

T model

The T model of the IM is shown in Fig. 2.1. The stator and rotor voltage equations in synchronous coordinates are given by

$$\boldsymbol{u}_\mathrm{s} = R_\mathrm{s}\boldsymbol{i}_\mathrm{s} + \frac{\mathrm{d}\boldsymbol{\psi}_\mathrm{s}}{\mathrm{d}t} + \omega_\mathrm{s}\boldsymbol{J}\boldsymbol{\psi}_\mathrm{s} \tag{2.3}$$

$$\boldsymbol{0} = R_\mathrm{r}\boldsymbol{i}_\mathrm{r} + \frac{\mathrm{d}\boldsymbol{\psi}_\mathrm{r}}{\mathrm{d}t} + \omega_\mathrm{r}\boldsymbol{J}\boldsymbol{\psi}_\mathrm{r} \tag{2.4}$$

where $\boldsymbol{\psi}_\mathrm{s}$ and $\boldsymbol{\psi}_\mathrm{r}$ are the stator flux linkage and the rotor flux linkage, respectively. The stator voltage vector is denoted by $\boldsymbol{u}_\mathrm{s}$, the stator current vector by $\boldsymbol{i}_\mathrm{s}$, and the stator resistance by R_s. The rotor current vector is $\boldsymbol{i}_\mathrm{r}$ and the rotor resistance is R_r. The angular slip frequency $\omega_\mathrm{r} = \omega_\mathrm{s} - \omega_\mathrm{m}$, where ω_m is the electrical angular speed of the rotor. The flux equations are

$$\boldsymbol{\psi}_\mathrm{s} = L_\mathrm{s}\boldsymbol{i}_\mathrm{s} + L_\mathrm{m}\boldsymbol{i}_\mathrm{r} \tag{2.5}$$

$$\boldsymbol{\psi}_\mathrm{r} = L_\mathrm{m}\boldsymbol{i}_\mathrm{s} + L_\mathrm{r}\boldsymbol{i}_\mathrm{r} \tag{2.6}$$

where the stator and rotor self-inductances are $L_\mathrm{s} = L_{\mathrm{s}\sigma} + L_\mathrm{m}$ and $L_\mathrm{r} = L_{\mathrm{r}\sigma} + L_\mathrm{m}$, respectively. The stator leakage inductance is denoted by $L_{\mathrm{s}\sigma}$, the rotor leakage inductance by $L_{\mathrm{r}\sigma}$, and the magnetizing inductance by L_m. The electromagnetic torque is given by

$$T_\mathrm{e} = \boldsymbol{i}_\mathrm{s}^\mathrm{T}\boldsymbol{J}\boldsymbol{\psi}_\mathrm{s} \tag{2.7}$$

where the matrix transpose is marked with the superscript T and per-unit quantities are used. The base values of per-unit system are defined as in Table 2.1.

The number of the inductances in the T model can be reduced to two as one leakage inductance is sufficient (Slemon, 1989). The simplified model can be either a Γ model or an inverse-Γ model.

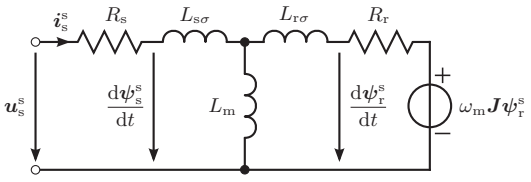

Figure 2.1. Dynamic T model of the IM in stator coordinates.

Table 2.1. Base values of per-unit system. U_N, I_N, and f_N are the rated values of line-to-line voltage, current and frequency, respectively.

Voltage u_B	$\sqrt{2/3}U_\mathrm{N}$
Current i_B	$\sqrt{2}I_\mathrm{N}$
Frequency f_B	f_N
Angular frequency ω_B	$2\pi f_\mathrm{N}$
Flux linkage ψ_B	$u_\mathrm{B}/\omega_\mathrm{B}$
Impedance Z_B	$u_\mathrm{B}/i_\mathrm{B}$
Inductance L_B	$Z_\mathrm{B}/\omega_\mathrm{B}$

Inverse-Γ *Model*

The inverse-Γ model in stator coordinates is shown in Fig. 2.2. The parameters and variables of the T model can be transformed into those of the inverse-Γ model using the factor

$$\gamma = \frac{L_\mathrm{m}}{L_\mathrm{r}} \tag{2.8}$$

as follows:

$$L_\mathrm{M} = \gamma L_\mathrm{m}, \quad L_\sigma = L_{\mathrm{s}\sigma} + \gamma L_{\mathrm{r}\sigma}, \quad R_\mathrm{R} = \gamma^2 R_\mathrm{r}, \quad \boldsymbol{\psi}_\mathrm{R} = \gamma \boldsymbol{\psi}_\mathrm{r}, \quad \boldsymbol{i}_\mathrm{R} = \boldsymbol{i}_\mathrm{r}/\gamma \tag{2.9}$$

The rotor voltage equation becomes

$$\mathbf{0} = R_\mathrm{R}\boldsymbol{i}_\mathrm{R} + \frac{\mathrm{d}\boldsymbol{\psi}_\mathrm{R}}{\mathrm{d}t} + \omega_\mathrm{r}\boldsymbol{J}\boldsymbol{\psi}_\mathrm{R} \tag{2.10}$$

The stator and rotor flux linkages are given by

$$\boldsymbol{\psi}_\mathrm{s} = (L_\sigma + L_\mathrm{M})\boldsymbol{i}_\mathrm{s} + L_\mathrm{M}\boldsymbol{i}_\mathrm{R} \tag{2.11}$$

$$\boldsymbol{\psi}_\mathrm{R} = L_\mathrm{M}(\boldsymbol{i}_\mathrm{s} + \boldsymbol{i}_\mathrm{R}) \tag{2.12}$$

respectively. The electromagnetic torque equation remains the same as (2.7). The inverse-Γ model is preferred for control purposes since it leads to simpler equations. The inverse-Γ model is applied in Publication IV and Publication V.

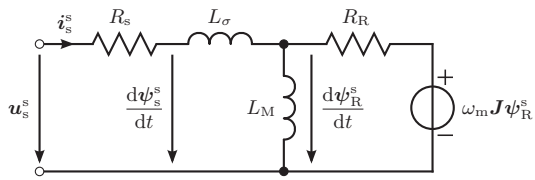

Figure 2.2. Dynamic inverse-Γ model of the IM in stator coordinates.

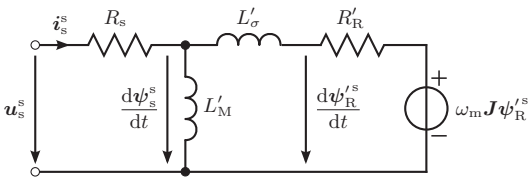

Figure 2.3. Dynamic Γ model of the IM in stator coordinates.

Γ *Model*

The Γ model in stator coordinates is shown in Fig. 2.3. The parameters and variables of the T model can be transformed to those of the Γ model using the factor

$$\gamma' = \frac{L_\mathrm{s}}{L_\mathrm{m}} \tag{2.13}$$

as follows:[1]

$$L'_\mathrm{M} = L_\mathrm{s}, \quad L'_\sigma = \gamma' L_{\mathrm{s}\sigma} + \gamma'^2 L_{\mathrm{r}\sigma}, \quad R'_\mathrm{R} = \gamma'^2 R_\mathrm{r}, \quad \boldsymbol{\psi}'_\mathrm{R} = \gamma' \boldsymbol{\psi}_\mathrm{r}, \quad \boldsymbol{i}'_\mathrm{R} = \boldsymbol{i}_\mathrm{r}/\gamma' \tag{2.14}$$

The rotor voltage equation becomes

$$\boldsymbol{0} = R'_\mathrm{R}\boldsymbol{i}'_\mathrm{R} + \frac{\mathrm{d}\boldsymbol{\psi}'_\mathrm{R}}{\mathrm{d}t} + \omega_\mathrm{r}\boldsymbol{J}\boldsymbol{\psi}'_\mathrm{R} \tag{2.15}$$

The stator and rotor flux linkages are given by

$$\boldsymbol{\psi}_\mathrm{s} = L'_\mathrm{M}(\boldsymbol{i}_\mathrm{s} + \boldsymbol{i}'_\mathrm{R}) \tag{2.16}$$

$$\boldsymbol{\psi}'_\mathrm{R} = \boldsymbol{\psi}_\mathrm{s} + L'_\sigma \boldsymbol{i}'_\mathrm{R} \tag{2.17}$$

respectively. The electromagnetic torque equation remains the same as (2.7). The Γ model is particularly suited for modeling the parameter variations rather than the inverse-Γ model (Slemon, 1989; Hinkkanen et al., 2006). The Γ model is applied in Publication I.

2.2.2 SyRM

The dynamic equivalent circuit of the SyRM in rotor coordinates is illustrated in Fig. 2.4. The d-axis of the rotating coordinate system is defined as the direction of the maximum inductance. The stator-voltage equation is

$$\boldsymbol{u}_\mathrm{s} = R_\mathrm{s}\boldsymbol{i}_\mathrm{s} + \frac{\mathrm{d}\boldsymbol{\psi}_\mathrm{s}}{\mathrm{d}t} + \omega_\mathrm{m}\boldsymbol{J}\boldsymbol{\psi}_\mathrm{s} \tag{2.18}$$

The stator current is

$$\boldsymbol{i}_\mathrm{s} = \boldsymbol{L}^{-1}\boldsymbol{\psi}_\mathrm{s} \tag{2.19}$$

[1] In Publication I, where only the Γ model is used, the prime of the notations was omitted.

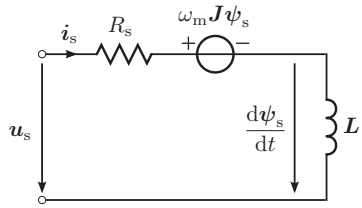

Figure 2.4. Dynamic model of an SyRM in rotor coordinates.

where the inductance matrix is

$$\boldsymbol{L} = \begin{bmatrix} L_\mathrm{d} & 0 \\ 0 & L_\mathrm{q} \end{bmatrix} \tag{2.20}$$

where L_d and L_q are the direct-axis and quadrature-axis inductances, respectively. The electromagnetic torque for per-unit quantities is

$$T_\mathrm{e} = \boldsymbol{i}_\mathrm{s}^\mathrm{T}\boldsymbol{J}\boldsymbol{\psi}_\mathrm{s} = i_\mathrm{q}\psi_\mathrm{d} - i_\mathrm{d}\psi_\mathrm{q} \tag{2.21}$$

where i_d and i_q represent the direct-axis and quadrature-axis components of the stator current, respectively.

2.3 Magnetic Saturation

The inductances of an electrical machine depend on the flux linkages (or the currents) due to magnetic saturation. When the current or flux is increased from zero, the inductance first increases slightly due to initial magnetic permeability, then the inductance drops due to saturation and gradually approaches a constant (fully saturated) level (Yamamoto et al., 2007). The saturation effects of the d-axis are more significant than those of the q-axis. There is coupling between the orthogonal axes, i.e., the d-axis inductance varies with not only the d-axis current but also with the q-axis current and vice versa (Vagati et al., 2000). Variation in the inductances can drastically affect loss-minimizing control and speed sensorless control in terms of precision and dynamics. Cross-saturation effects are usually more significant in SyRMs than those in IMs. This section investigates the magnetic saturation of the SyRM.

The inductance value cannot be measured directly, i.e., only the stator current, the stator voltage and the rotor speed are measurable. Usually, the inductances are identified using measurements (Armando et al., 2013) or finite-element methods (Zhao et al., 2011). The results are used to generate a look-up table or fitted to an approximate function. Explicit functions are preferable because they are convenient in numerical analyses

and simulations and can also be easily embedded in dynamic equivalent circuits. Explicit function models do not need to store the measured inductances and they are continuous and differentiable, contrary to look-up tables.

In some applications, a very simple saturation model may suffice. Mademlis (2003) models the d-axis inductance using a piecewise function which divides the saturation curve into two linear parts. Piecewise functions can simplify the mathematical expressions. However, they are not differentiable on the boundary and lead to large fitting errors. Polynomial functions have been used in (Kilthau and Pacas, 2002) and the coefficients are determined using the method of least squares. This model takes into account cross-saturation effects. The accuracy of polynomial fitting depends on the degree of the polynomial. The main disadvantage of the polynomial model is that the accuracy significantly deteriorates outside the range of the data. A modified arctangent function has been also used in earlier work (Corzine et al., 1998; Plexim GmbH, 2012). The parameters of this model have physical interpretation, leading to comparatively an easy fitting procedure. However, these models have not taken into account cross saturation. Yamamoto et al. (2007) proposed a saturation model using modified rational functions. This model takes cross saturation into account and yields good fitting results, though their model requires 16 parameters.

Publication II proposed a modified power function model. The purpose was to develop an explicit function model that 1) fits well to the saturation curves; 2) keeps the number of parameters small; 3) takes cross-saturation effects into account; 4) fulfills the reciprocity condition; and 5) leads to an easy fitting procedure. The starting point for developing the saturation model is a simple power function model proposed by de Jong (1980)

$$i_{\mathrm{d}}(\psi_{\mathrm{d}}) = \frac{\psi_{\mathrm{d}}}{L_{\mathrm{du}}}\left[1 + (\alpha|\psi_{\mathrm{d}}|)^a\right] \tag{2.22}$$

where L_{du} is the unsaturated inductance and α and a are nonnegative constants. This simple model was found to accurately represent the saturation characteristic if cross saturation is omitted. The conservation of energy leads to the reciprocity condition (Chua, 1980; Melkebeek and Willems, 1990; Sauer, 1992; Vagati et al., 2000)

$$\frac{\partial \psi_{\mathrm{d}}}{\partial i_{\mathrm{q}}} = \frac{\partial \psi_{\mathrm{q}}}{\partial i_{\mathrm{d}}}, \tag{2.23}$$

In Publication II, the function (2.22) was modified in order to take cross

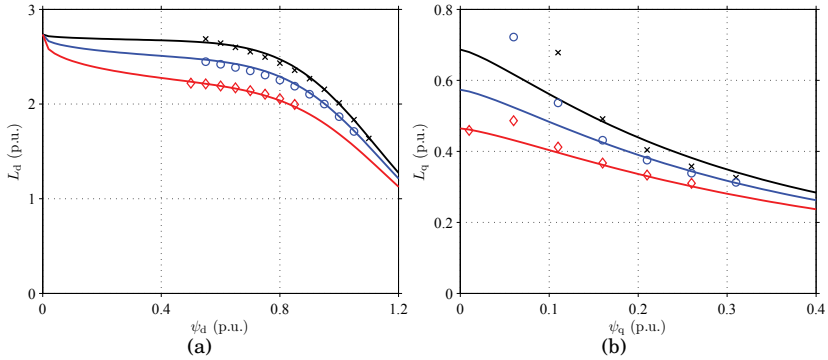

Figure 2.5. Results of experimental data fitting: (a) L_d as a function of ψ_d for three different values of ψ_q: 0.1 p.u. (black line), 0.2 p.u. (blue line) and 0.3 p.u. (red line); (b) L_q as a function of ψ_q for three different values of ψ_d: 0.6 p.u. (black line), 0.8 p.u. (blue line) and 1.0 p.u. (red line).

saturation into account while fulfilling the reciprocity condition (2.23). In order to develop explicit functions which fulfill the reciprocity condition, functions of the following form can be considered (Vagati et al., 2000):

$$i_\mathrm{d}(\psi_\mathrm{d},\psi_\mathrm{q}) = i_\mathrm{d}(\psi_\mathrm{d},0) + \frac{\mathrm{d}f(\psi_\mathrm{d})}{\mathrm{d}\psi_\mathrm{d}} g(\psi_\mathrm{q}) \tag{2.24a}$$

$$i_\mathrm{q}(\psi_\mathrm{d},\psi_\mathrm{q}) = i_\mathrm{q}(0,\psi_\mathrm{q}) + f(\psi_\mathrm{d}) \frac{\mathrm{d}g(\psi_\mathrm{q})}{\mathrm{d}\psi_\mathrm{q}} \tag{2.24b}$$

where the first terms $i_\mathrm{d}(\psi_\mathrm{d},0)$ and $i_\mathrm{q}(0,\psi_\mathrm{q})$ are the currents in no-load conditions. It can be easily seen that these functions fulfill (2.23). Augmenting the power function with $f(\psi_\mathrm{d}) \propto \psi_\mathrm{d}^{c+2}$ and $g(\psi_\mathrm{q}) \propto \psi_\mathrm{q}^{d+2}$ yields the modified power function model proposed in Publication II:

$$i_\mathrm{d}(\psi_\mathrm{d},\psi_\mathrm{q}) = \frac{\psi_\mathrm{d}}{L_\mathrm{du}} \left[1 + (\alpha|\psi_\mathrm{d}|)^a + \frac{\gamma L_\mathrm{du}}{d+2} |\psi_\mathrm{d}|^c |\psi_\mathrm{q}|^{d+2} \right] \tag{2.25a}$$

$$i_\mathrm{q}(\psi_\mathrm{d},\psi_\mathrm{q}) = \frac{\psi_\mathrm{q}}{L_\mathrm{qu}} \left[1 + (\beta|\psi_\mathrm{q}|)^b + \frac{\gamma L_\mathrm{qu}}{c+2} |\psi_\mathrm{d}|^{c+2} |\psi_\mathrm{q}|^d \right] \tag{2.25b}$$

where L_du and L_qu are the unsaturated inductances, and α, β, γ, a, b, c, and d are nonnegative constants. The model has nine parameters in total. The modified power functions are physically consistent and can preserve the saturation characteristics outside the range of data. The models using rational functions or polynomial functions do not have this property. Even though they can fit well to the data, the fitting results can lead to infinite or negative inductance values outside the range of data.

The measured inductance data and the curves from the fitted functions are shown in Fig. 2.5. The d-axis inductance L_d is shown as a function of ψ_d for three different values of ψ_q in Fig. 2.5(a). A similar representation for the q-axis inductance L_q is used in Fig. 2.5(b). It can be seen that the function (2.25) fits very well to the measured data.

3. Loss Minimization

The losses in the motors can be reduced using loss minimization methods, which can be divided into two categories: loss-model based controllers and online search controllers. The loss-model based controllers model the losses as functions of motor parameters and operating conditions. The efficiency-optimal control variable is calculated by minimizing the total loss function. The online search methods adjust the control variable based on the feedback of the input power measurements. The online search controllers typically have slow convergence and can cause torque disturbances (Bazzi and Krein, 2010). This dissertation focuses on loss-model based methods. Loss-minimizing methods for IMs have been reviewed in (Abrahamsen et al., 1998; Vukosavic and Levi, 2003; Bazzi and Krein, 2010) and those for SyRMs are reviewed in Publication III. In order to obtain an analytical solution, conventional methods usually omit saturation effects or use a very simple saturation model, thereby simplifying the loss function by omitting hysteresis losses. The inaccuracy of the loss model and inductances will cause deviation from the ideal maximum efficiency points.

This dissertation proposes loss-minimizing controllers for IMs and SyRMs, which take into account both hysteresis losses and saturation effects. The loss-minimizing controllers are evaluated in terms of their parameter sensitivity and dynamic performance. This chapter briefly introduces the loss-minimizing method for IM proposed in Publication I.

3.1 Copper Losses and Core Losses

The main losses in an electrical machine are result from copper losses and core losses. Copper losses represent the ohmic losses in the winding as the current flows through the winding. Copper losses dominate when the load

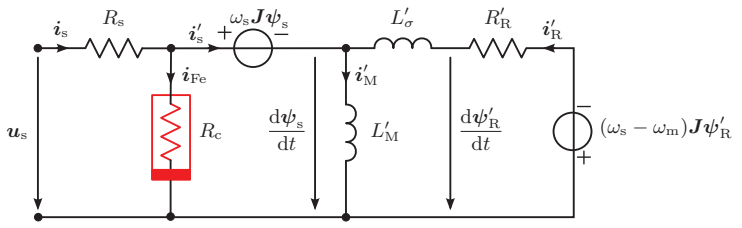

Figure 3.1. Dynamic Γ model of the IM in synchronous coordinates with the core-loss resistance.

is high. For the Γ model of the IM, the copper losses can be expressed as

$$P_{\mathrm{Cu}} = R_s i_s^2 + R'_R i'^2_R \tag{3.1}$$

where per-unit quantities are assumed. The magnitudes of the stator current and rotor current are denoted by $i_s = \|\boldsymbol{i}_s\|$ and $i'_R = \|\boldsymbol{i}'_R\|$, respectively. The magnitudes of other vector quantities are denoted similarly. Core losses represent the losses in the motor due to varying flux in the magnetic material. They can mainly be classified into hysteresis losses and eddy-current losses. Eddy-current losses are due to circular currents induced by the varying magnetic field, while hysteresis losses are the energy consumed in magnetizing and demagnetizing a magnetic material (Shultz, 1997). The core losses at low frequencies (in the range of fundamental frequencies) can be modeled as

$$P_{\mathrm{Fe}} = G_{\mathrm{Ft}}\omega_s^2\psi_s^2 + \Lambda_{\mathrm{Hy}}|\omega_s|\psi_s^2 \tag{3.2}$$

where the first term corresponds to the eddy-current losses and the second term corresponds to the hysteresis losses. The constants G_{Ft} and Λ_{Hy} determine the ratio between the loss components at a given stator flux and angular frequency. They can be identified using no-load tests at different frequencies and flux levels.

Copper losses and core losses represent particularly the main losses for the purpose of loss minimization, since other losses are independent of control, or their effects are minor.

3.2 Loss Minimization Algorithm

The dynamic Γ model of the IM, including the core-loss resistance, is shown in Fig. 3.1. The core-loss resistance in the steady state is

$$R_c = \frac{1}{\Lambda_{\mathrm{Hy}}/|\omega_s| + G_{\mathrm{Ft}}} \tag{3.3}$$

Generally, the effect of cross saturation is minor in the case of typical IMs. Therefore, a simplified magnetic saturation model (de Jong, 1980; Vukosavic and Levi, 2003) is used in loss-minimizing control:

$$L_{\mathrm{M}}(\psi_{\mathrm{s}}) = \frac{L_{\mathrm{u}}}{1 + (\beta\psi_{\mathrm{s}})^S} \tag{3.4}$$

where L_{u} is the unsaturated inductance, and S and β are nonnegative constants. These parameters can be identified using a series of no-load tests at different voltage levels.

The basic principle of the loss-model based controller is minimize the total copper losses and core losses under the constraints of maximum voltage and current limits. If the rotor flux magnitude ψ'_{R} is selected as the loss-minimizing control variable, the power-loss function should be formulated as

$$P_{\mathrm{loss}} = f(T_{\mathrm{e}}, \omega_{\mathrm{s}}, \psi'_{\mathrm{R}}) \tag{3.5}$$

This function can be derived by equations based on the dynamic Γ model of the IM.

The total losses should be minimized, while the electromagnetic torque and the rotor speed should be controlled to their desired values. At each sampling period, the given rotor speed and torque are assumed to be constant parameters. Due to nonlinear inductance and core-loss resistance, the mathematical expression of the loss function is complicated, and the analytical solution of ψ'_{R} which minimizes P_{loss} cannot be derived. However, the loss-minimizing rotor flux can be determined using a minimum searching method, e.g., the golden section method. Due to the rotor time constant, the reduced rotor flux will result in a slow dynamic response. In order to speed up the rotor-flux dynamics, a proportional flux controller with a feedforward term was proposed in Publication I. The loss-minimizing flux control is integrated with a voltage feedback field-weakening algorithm to provide smooth transitions between the loss-minimizing region at low speeds, and the voltage-feedback field-weakening region at higher speeds.

3.3 Experimental Validation

The proposed loss-minimizing flux controller improves energy efficiency at the steady state. Fig. 3.2 shows the experimental results of the loss-minimizing flux control and constant-flux control. Comparison of the loss measurements for the two controllers showed that the proposed method

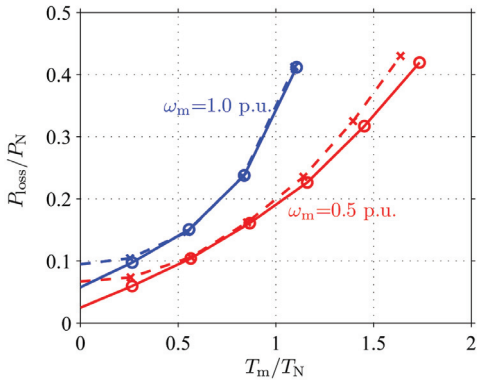

Figure 3.2. Experimental results showing the total losses of the 2.2-kW IM using proposed loss-minimizing control (solid line) and constant-flux control (dashed line). T_{m} is the measured mechanical torque.

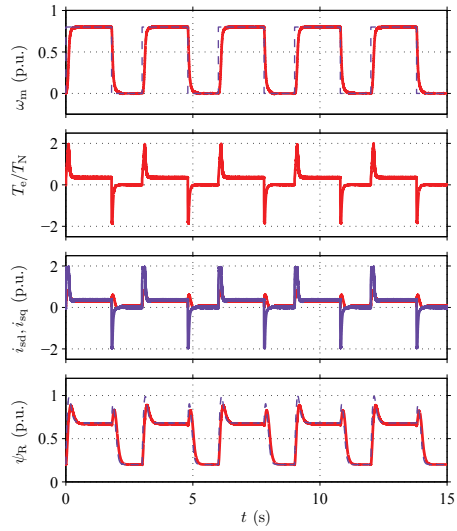

Figure 3.3. S5 duty cycles. The cycle duration is 3 s.

significantly reduces the steady-state losses in low-load and over-load operations. The proposed loss-minimizing controller was also investigated for dynamic applications. Intermittent periodic duty with acceleration and electric breaking (IEC duty type S5) was carried out in experiments. The duty cycles with cycle duration of 3 s are shown in Fig. 3.3. The measured input power for different cycle durations between 1 s and 7 s is shown in Fig. 3.4. In the case of the shortest cycle durations, the current required for changing the flux in accelerations and decelerations contributes to the losses so much that the constant-flux operation becomes more beneficial.

Publication IV proposed a loss-minimizing controller for SyRMs. The

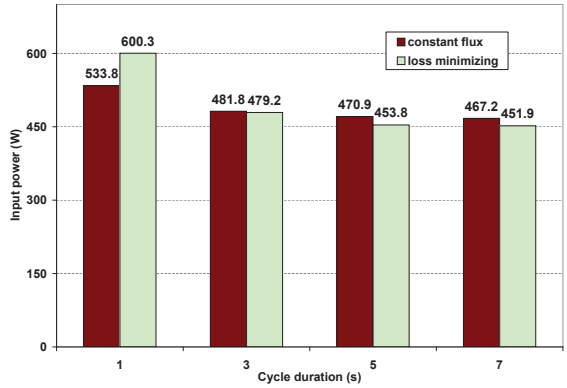

Figure 3.4. Input power measurement of S5 duty cycles.

principle underlying loss minimization in SyRMs is similar to that in IMs. However, the saturation effects of SyRMs are more significant than those of IMs. The saturation effects are modeled using the model proposed in Publication II, which takes into account cross saturation. Since this model is more complicated, searching for the loss-minimizing point becomes too computationally demanding for real-time control. Instead of calculating the loss-minimizing point in real time, the optimal control variable is calculated offline and fitted to a simple function for online implementation. For SyRMs, torque dynamics can be maintained even with a reduced flux level because the flux is directly proportional to the stator current, contrary to IMs.

4. Flux Observers for IMs

Field-oriented control of IMs requires knowing the position of the rotor flux. Measuring the physical rotor position of IMs does not yield the rotor flux angle because of the slip. It is therefore necessary to apply a flux estimator, which can be either a speed-sensored estimator or a speed-sensorless estimator. Generally, an electric drive without a speed sensor installed is preferred, since eliminating the sensor can reduce the overall cost of the setup. This makes the mechanical setup and maintenance less troublesome, and improves the reliability, especially in hostile environments.

Flux estimators are typically based on the standard dynamic motor model which relies on the motor parameters. At the lowest speeds, the back-electromotive force induced by the rotational movement of the rotor is extremely small, and the influences of parameter errors and measurement errors become critical. The flux estimator is also severely affected by the nonlinearities of the inverter at the lowest speeds, thus the performance of flux estimators deteriorates at low speeds. Although various flux estimation methods have been proposed, most of these fail to solve the stability problem at low speeds.

This chapter describes the flux estimators for IMs, reviews different flux estimation methods, as well as discusses their stability and performance. The gains of the closed-loop flux estimators can be properly selected to improve stability. It is also possible to vary the gains as functions of the operating speed to achieve a desired damping of the estimation error dynamics. The gain scheduling method for a speed-adaptive full-order flux observer was proposed in Publication V.

4.1 Voltage Model

The integration of the stator voltage equation gives the traditional voltage model flux estimator. The main advantage of the voltage model is that the speed is not present in the equation, thus making it an inherently sensorless flux estimator. However, the voltage model is sensitive to the parameter error of the stator resistance in the low-speed region, where the signal-to-noise ratio of the stator voltage measurement is very poor and voltage drop in the stator resistance is dominant. Furthermore, the pure open-loop integrator in the voltage model is marginally stable, and offset in the current measurement will cause drift at all frequencies. To solve the drift problem, the pure integrator can be replaced by a low-pass filter (Takahashi and Noguchi, 1986; Hurst et al., 1998). The low-pass filter induces a steady-state error into the estimate, which must be compensated for by a compensation term (Shin et al., 2000; Hinkkanen and Luomi, 2003). Bose and Patel (1997) proposed programmable low-pass filters which select the filter bandwidth proportional to the stator frequency. The modified voltage models are very simple. However, the inherent parameter sensitivity properties of the voltage model still remain. Voltage models are known to be sensitive to stator resistance variation, inverter nonlinearity and measurement errors at low speeds. Therefore they fail to provide satisfactory performance at the lowest speeds.

4.2 Reduced-Order Observer

The standard method in control theory for estimating non-measurable state variables is to apply a full-order observer. However, since the stator current is a measurable quantity, there is no immediate need for calculating an estimate thereof. Rather, a reduced-order observer can be constructed. The observer developed by Ohtani et al. (1992) can be seen as a simplified inherently sensorless reduced-order observer. A typical reduced-order flux observer have been used in previous work (Verghese and Sanders, 1988; Harnefors, 2001; Hinkkanen et al., 2010). The observer structure in estimated rotor flux coordinates can be expressed as

$$\frac{\mathrm{d}\hat{\boldsymbol{\psi}}_\mathrm{R}}{\mathrm{d}t} + \hat{\omega}_\mathrm{s}\boldsymbol{J}\hat{\boldsymbol{\psi}}_\mathrm{R} = \boldsymbol{e} + \boldsymbol{G}(\hat{\boldsymbol{e}} - \boldsymbol{e}) \tag{4.1}$$

where $\boldsymbol{G}$ is the observer gain matrix, and symbols with circumflex denote estimates. The two expressions for the back EMF induced by the rotor flux

are

$$\boldsymbol{e} = \boldsymbol{u}_\mathrm{s} - \hat{R}_\mathrm{s}\boldsymbol{i}_\mathrm{s} - \hat{L}_\sigma \frac{\mathrm{d}\boldsymbol{i}_\mathrm{s}}{\mathrm{d}t} - \hat{\omega}_\mathrm{s} L_\sigma \boldsymbol{J}\boldsymbol{i}_\mathrm{s} \tag{4.2a}$$

$$\hat{\boldsymbol{e}} = \hat{R}_\mathrm{R}\boldsymbol{i}_\mathrm{s} - \left(\frac{\hat{R}_\mathrm{R}}{\hat{L}_\mathrm{M}}\boldsymbol{I} - \omega_\mathrm{m}\boldsymbol{J}\right)\hat{\boldsymbol{\psi}}_\mathrm{R} \tag{4.2b}$$

where the identity matrix is $\boldsymbol{I} = \left[\begin{smallmatrix}1 & 0\\ 0 & 1\end{smallmatrix}\right]$. If the gain of the reduced-order observer $\boldsymbol{G}$ is selected to be a zero matrix, the pure voltage model is obtained (Hinkkanen et al., 2010), and if $\boldsymbol{G}$ is selected to be $\boldsymbol{I}$, the current model is obtained. The current model is a speed-sensored flux estimator, since it requires the rotor speed. As a speed-sensored estimator, it is known to give stable operation in the low-speed region (Harnefors and Hinkkanen, 2014). The current model is sensitive to $\hat{R}_\mathrm{R}$ and $\hat{L}_\mathrm{M}$ at high frequencies (Jansen and Lorenz, 1994). It has been suggested that the current model observer be used at low speed and the voltage model at high speeds (Jansen and Lorenz, 1994; Jansen et al., 1994). The reduced-order observer inherently combines the voltage model and the current model which could complement one another.

In order to make the observer independent of the rotor speed estimate, the observer gain matrix was selected as

$$\boldsymbol{G} = \frac{\boldsymbol{G}'\hat{\boldsymbol{\psi}}_\mathrm{R}\hat{\boldsymbol{\psi}}_\mathrm{R}^\mathrm{T}}{\hat{\psi}_\mathrm{R}^2} \tag{4.3}$$

where $\boldsymbol{G}' = g_\mathrm{d}\boldsymbol{I} + g_\mathrm{q}\boldsymbol{J}$ is a gain matrix. With this gain selection, the term proportional to ω_m in (4.2b) vanishes. An approximate relationship has been derived between the reduced-order and full-order observer gains in (Harnefors and Hinkkanen, 2008). This reduced-order observer was used as a benchmark method in Publication V, and the general stabilizing gain selection proposed in (Hinkkanen et al., 2010) was applied.

4.3 Speed-Adaptive Full-Order Observer

4.3.1 Observer Structure

The speed-adaptive full-order observer proposed by Kubota et al. (1993) is expressed as

$$\frac{\mathrm{d}\hat{\boldsymbol{x}}}{\mathrm{d}t} = \hat{\boldsymbol{A}}\hat{\boldsymbol{x}} + \boldsymbol{B}\boldsymbol{u}_\mathrm{s} + \boldsymbol{K}(\boldsymbol{i}_\mathrm{s} - \hat{\boldsymbol{i}}_\mathrm{s}) \tag{4.4a}$$

$$\hat{\boldsymbol{i}}_\mathrm{s} = \boldsymbol{C}\hat{\boldsymbol{x}} \tag{4.4b}$$

The state estimate vector is

$$\hat{\boldsymbol{x}} = \begin{bmatrix} \hat{\boldsymbol{i}}_{\mathrm{s}} \\ \hat{\boldsymbol{\psi}}_{\mathrm{R}} \end{bmatrix} \tag{4.5}$$

and the system matrices are

$$\hat{\boldsymbol{A}} = \begin{bmatrix} -\frac{\hat{R}_\sigma}{\hat{L}_\sigma}\boldsymbol{I} - \hat{\omega}_{\mathrm{s}}\boldsymbol{J} & \frac{1}{\hat{L}_\sigma}(\frac{\hat{R}_{\mathrm{R}}}{\hat{L}_{\mathrm{M}}}\boldsymbol{I} - \hat{\omega}_{\mathrm{m}}\boldsymbol{J}) \\ \hat{R}_{\mathrm{R}}\boldsymbol{I} & -\frac{\hat{R}_{\mathrm{R}}}{\hat{L}_{\mathrm{M}}}\boldsymbol{I} - (\hat{\omega}_{\mathrm{s}} - \hat{\omega}_{\mathrm{m}})\boldsymbol{J} \end{bmatrix}, \quad \hat{\boldsymbol{B}} = \begin{bmatrix} \frac{1}{\hat{L}_\sigma}\boldsymbol{I} \\ \boldsymbol{O} \end{bmatrix}, \quad \boldsymbol{C} = \begin{bmatrix} \boldsymbol{I} & \boldsymbol{O} \end{bmatrix} \tag{4.6}$$

where the total resistance estimate is $\hat{R}_\sigma = \hat{R}_{\mathrm{s}} + \hat{R}_{\mathrm{R}}$. The observer gain matrix is

$$\boldsymbol{K} = \begin{bmatrix} \boldsymbol{K}_{\mathrm{s}} \\ \boldsymbol{K}_{\mathrm{r}} \end{bmatrix} = \begin{bmatrix} k_{\mathrm{sd}}\boldsymbol{I} + k_{\mathrm{sq}}\boldsymbol{J} \\ k_{\mathrm{rd}}\boldsymbol{I} + k_{\mathrm{rq}}\boldsymbol{J} \end{bmatrix} \tag{4.7}$$

The rotor speed estimate is obtained using the conventional adaptation law

$$\hat{\omega}_{\mathrm{m}} = k_{\mathrm{p}}\hat{\boldsymbol{\psi}}_{\mathrm{R}}^{\mathrm{T}}\boldsymbol{J}\tilde{\boldsymbol{i}}_{\mathrm{s}} + \int k_{\mathrm{i}}\hat{\boldsymbol{\psi}}_{\mathrm{R}}^{\mathrm{T}}\boldsymbol{J}\tilde{\boldsymbol{i}}_{\mathrm{s}}\mathrm{d}t \tag{4.8}$$

where k_{p} and k_{i} are the speed adaptation gains. The current estimation error $\tilde{\boldsymbol{i}}_{\mathrm{s}} = \boldsymbol{i}_{\mathrm{s}} - \hat{\boldsymbol{i}}_{\mathrm{s}}$, and estimation errors of other variables are marked similarly.

4.3.2 Observer Gain Selection

The selection of the observer gains can be a difficult task. Large observer gains result in faster convergence. However, as the observer gains are increased, the sensitivity to noise increases as well. The classical approach to observer gain selection is to design the observer poles proportional to the motor poles (Kubota et al., 1993). It was found that the adaptive observer is unstable in a small area in regenerating mode at low speeds. Kubota et al. (2002) improved the gain design by selecting the proportional constant as a function of stator frequency and rotor speed in the regenerating mode. Harnefors (1997) proposed a gain selection that yields well-damped and comparatively robust estimation-error dynamics at higher speeds. However, the drawback of this gain selection is that it results in an unstable region at low speeds in the regenerating mode (Harnefors and Hinkkanen, 2008).

Sangwongwanich et al. (2007) proposed general stabilizing observer gains

$$\boldsymbol{K}_{\mathrm{s}} = \frac{r - \hat{R}_{\sigma}}{\hat{L}_{\sigma}}\boldsymbol{I} + \frac{x}{\hat{L}_{\sigma}}\boldsymbol{J} \tag{4.9a}$$

$$\boldsymbol{K}_{\mathrm{r}} = \left(\hat{R}_{\mathrm{R}} - r + \frac{\hat{R}_{\mathrm{R}}}{\hat{L}_{\mathrm{M}}}l\right)\boldsymbol{I} + (\hat{\omega}_{\mathrm{m}}l - x)\boldsymbol{J} \tag{4.9b}$$

where $l > 0$, $r > 0$, and x can be freely chosen. With these gains, the closed-loop estimation error dynamics are locally stable in any operating point (for positive k_{p} and k_{i}). The three free parameters l, r, and x can be selected as functions of the speed estimate (or the stator frequency). However, the selection of the three parameters in (Sangwongwanich et al., 2007) results in dynamics of the observer equivalent to those of the pure voltage model at zero frequency. Chen et al. (2014) proposed a feedback gain selection based on the speed convergence rate, which satisfies general stabilizing conditions (4.9). In the low-speed operating region, the gains are selected to eliminate the unstable area, and zero gains are adopted in the other operating region below the rated speed. However, the zero observer gains may cause problems at high speeds due to poor damping (Hinkkanen, 2004).

The key contribution of Publication V is a proposed gain design method based on the general stabilizing observer gain design framework presented in (Sangwongwanich et al., 2007). The gains are scheduled for the entire operating speed region. The three design parameters l, r, and x are selected so that the observer gains at higher speeds resemble those in (Harnefors, 1997), while avoiding the voltage-model behavior of those in (Sangwongwanich et al., 2007). Furthermore, a resistance adaptation law was applied to improve the stability when operating at low speed. The stator-resistance adaptation gain is linearly reduced with the increase of $\hat{\omega}_{\mathrm{s}}$ to gradually disable the adaptation at high speeds due to the poor signal-to-noise ratio of stator-resistance estimation at higher stator frequencies. The proposed observer design has led to a completely stable, well-damped, and comparatively robust system.

5. Discrete Current Control

Controllers in the electric drives are implemented in a digital processor instead of analog electronics. The controller can be designed in the continuous-time domain and discretized using, e.g., Euler's or Tustin's methods, commonly referred to as emulation. Usually the emulation design can achieve good performance if the sampling frequency is high. However, the discrete controller based on the continuous design may encounter limitations due to sampling and delays (Yim et al., 2009). When the fundamental-to-sampling frequency ratio is high, the discrete controller has poor performance or even instabilities. In order to achieve good performance, the controller can be designed in the discrete domain and be based on a discrete model. This chapter presents the discrete current control design proposed in Publication VI, which is suitable for SyRMs. An exact discrete model of the SyRM and the current controller based on the exact model are briefly introduced.

5.1 Exact Discrete-Time Model

The state-space representation of the SyRM in rotor coordinates is

$$\frac{\mathrm{d}\boldsymbol{\psi}_\mathrm{s}(t)}{\mathrm{d}t} = \boldsymbol{A}\boldsymbol{\psi}_\mathrm{s}(t) + \boldsymbol{B}\boldsymbol{u}_\mathrm{s}(t) \tag{5.1a}$$

$$\boldsymbol{i}_\mathrm{s}(t) = \boldsymbol{C}\boldsymbol{\psi}_\mathrm{s}(t) \tag{5.1b}$$

The system matrices are

$$\boldsymbol{A} = \begin{bmatrix} -R_\mathrm{s}/L_\mathrm{d} & \omega_\mathrm{m} \\ -\omega_\mathrm{m} & -R_\mathrm{s}/L_\mathrm{q} \end{bmatrix}, \quad \boldsymbol{B} = \boldsymbol{I}, \quad \boldsymbol{C} = \begin{bmatrix} 1/L_\mathrm{d} & 0 \\ 0 & 1/L_\mathrm{q} \end{bmatrix} \tag{5.2}$$

The exact closed-form discrete-time model for SyRMs in rotor coordinates has been derived assuming that the ZOH of the stator voltage is in stator coordinates. This assumption is physically well justified. The rotor speed

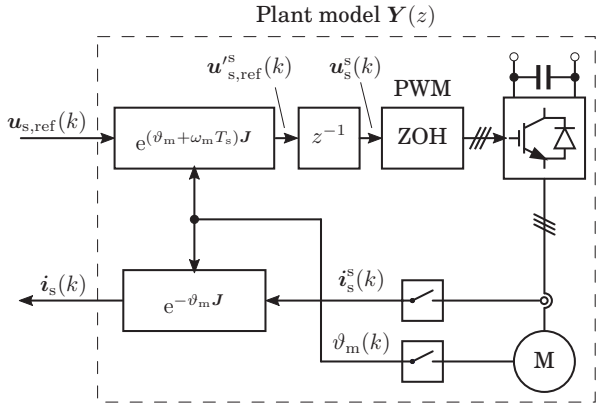

Figure 5.1. Discrete-time modeling of a converter-fed SyRM drive. The sampling of the stator currents is assumed to be synchronized with the PWM. The model incudes the effects of the ZOH in stator coordinates, coordinate transformations, and computational time delay z^{-1}.

and the motor parameters are assumed to be quasi-constants. Sampling of the stator currents is assumed to be synchronized with the PWM. The sampling used averaged quantities in the switching-cycle. Under these assumptions, the stator voltage is piecewise constant in stator coordinates between the two consecutive sampling instants, which corresponds to a zero-order hold (ZOH) in stator coordinates.

The discrete-time state-space representation is given by

$$\boldsymbol{\psi}_{\mathrm{s}}(k+1) = \boldsymbol{\Phi}\boldsymbol{\psi}_{\mathrm{s}}(k) + \boldsymbol{\Gamma}\boldsymbol{u}_{\mathrm{s}}(k) \tag{5.3a}$$

$$\boldsymbol{i}_{\mathrm{s}}(k) = \boldsymbol{C}\boldsymbol{\psi}_{\mathrm{s}}(k) \tag{5.3b}$$

where $\boldsymbol{\Phi}$, $\boldsymbol{\Gamma}$, and $\boldsymbol{C}$ are the discrete-time system matrices. The discrete-time state matrix is

$$\boldsymbol{\Phi} = \mathrm{e}^{\boldsymbol{A}T_{\mathrm{s}}} \tag{5.4}$$

The discrete-time input matrix becomes

$$\boldsymbol{\Gamma} = \int_0^{T_{\mathrm{s}}} \mathrm{e}^{\boldsymbol{A}\tau}\mathrm{e}^{-\omega_{\mathrm{m}}(T_{\mathrm{s}}-\tau)\boldsymbol{J}}\mathrm{d}\tau \tag{5.5}$$

If the stator current is chosen as a state variable, the state equation can be expressed as

$$\boldsymbol{i}_{\mathrm{s}}(k+1) = \boldsymbol{F}\boldsymbol{i}_{\mathrm{s}}(k) + \boldsymbol{G}\boldsymbol{u}_{\mathrm{s}}(k) \tag{5.6}$$

where the new system matrices are

$$\boldsymbol{F} = \boldsymbol{C}\boldsymbol{\Phi}\boldsymbol{C}^{-1}, \quad \boldsymbol{G} = \boldsymbol{C}\boldsymbol{\Gamma} \tag{5.7}$$

These discrete-time matrices provide the mapping between the continuous-time model (with physical parameters) and the discrete-time model. The discrete-time modeling of the SyRM drive is shown in Fig. 5.1.

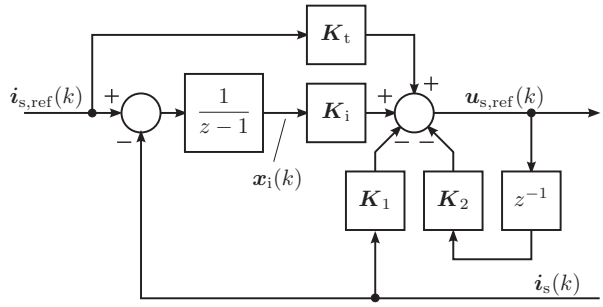

Figure 5.2. 2DOF state-space current controller with an integral action. The gains $\boldsymbol{K}_1$, $\boldsymbol{K}_2$, $\boldsymbol{K}_\mathrm{i}$, and $\boldsymbol{K}_\mathrm{t}$ are 2×2 matrices.

5.2 Discrete-Time Controller

Harnefors and Nee (1998) proposed a model-based current controller of AC motor using the internal model control method. The controller parameters are expressed using only the motor parameters and the desired closed-loop bandwidth. The tuning of the controller gains was simplified to select only the control bandwidth. The discrete-time controller proposed in Publication VI can be seen as a counterpart of the control design in the discrete-time domain.

The proposed control law is

$$\boldsymbol{x}_\mathrm{i}(k+1) = \boldsymbol{x}_\mathrm{i}(k) + \boldsymbol{i}_{\mathrm{s,ref}}(k) - \boldsymbol{i}_\mathrm{s}(k) \tag{5.8a}$$

$$\boldsymbol{u}_{\mathrm{s,ref}}(k) = \boldsymbol{K}_\mathrm{t}\boldsymbol{i}_{\mathrm{s,ref}}(k) + \boldsymbol{K}_\mathrm{i}\boldsymbol{x}_\mathrm{i}(k) - \boldsymbol{K}_1\boldsymbol{i}_\mathrm{s}(k) - \boldsymbol{K}_2\boldsymbol{u}_\mathrm{s}(k) \tag{5.8b}$$

where $\boldsymbol{x}_\mathrm{i}$ is the integral state, $\boldsymbol{K}_\mathrm{i}$ is the integral gain, $\boldsymbol{K}_\mathrm{t}$ is the feedforward gain, $\boldsymbol{K}_1$ and $\boldsymbol{K}_2$ are the state-feedback gains, and $\boldsymbol{u}_\mathrm{s}(k+1) = \boldsymbol{u}_{\mathrm{s,ref}}(k)$. The discrete controller is shown in Fig. 5.2.

5.2.1 Stability Analysis

The robustness of the proposed current controller has been analyzed against errors of the three parameters L_d, L_q, and R_s. One of the actual parameters is varied in a range from 0 to 2.5 times the estimate value, and the other two parameters match with their estimates. The controller gains are calculated using the parameter estimates. The eigenvalues of the closed-loop system are calculated for the bandwidth α_c in a range from 0 to $2\pi{\cdot}500$ rad/s. Four different designs are evaluated:

Design 1: approximation of the continuous-time design using the Euler method;

Design 2: proposed design based on the approximate model with $\boldsymbol{\Psi} = \boldsymbol{I}$;

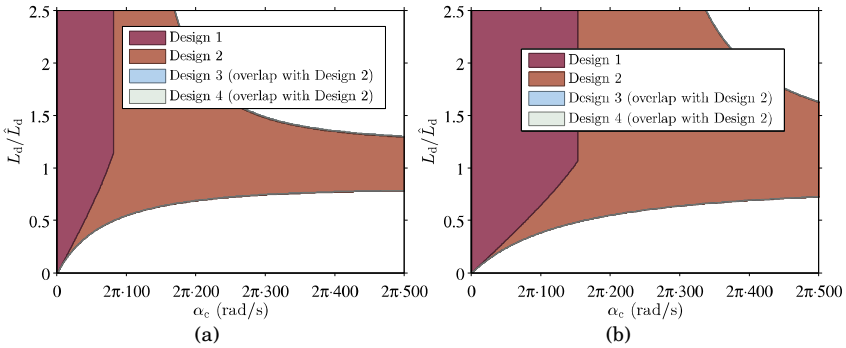

Figure 5.3. Stability maps as a function of the desired bandwidth α_c and the ratio $L_d/\hat{L}_d$. The electrical angular frequency is 0 Hz and the sampling frequencies are 1 kHz (a) and 2 kHz (b).

Design 3: proposed design based on the approximate model with $\boldsymbol{\Psi} = \boldsymbol{I} + (T_s/2)\boldsymbol{A}$;

Design 4: proposed discrete-time design based on the exact model.

The following results examine three different electrical angular frequencies of 0 Hz, 100 Hz and 200 Hz, and two different sampling frequencies of 1 kHz and 2 kHz.

Fig. 5.3 shows the stability maps at zero speed as a function of the desired bandwidth α_c and the ratio $L_d/\hat{L}_d$. It can be seen that the proposed design based on the exact model has the same stable region as those based on the approximate models, while the continuous-time design has a comparatively smaller stable region than those of the other designs. It can be seen that increasing the sampling frequency from 1 kHz to 2 kHz expands the stable region of all these designs. Fig. 5.4 shows the results at an electrical angular frequency of 100 Hz. As the operating frequency increases, differences emerge between the designs using the exact model and approximate models. It can be seen that Design 3 has an overlapped stable region with that of the proposed design based on the exact model. The results at a 200-Hz electrical angular frequency are shown in Fig. 5.5. It can be seen from Fig. 5.5(a) that when the sampling frequency is 1 kHz, Design 1 has no stable region at all. The stable region of Design 2 is very small and those of Design 3 and 4 are comparatively large. Based on the stability analysis of L_q, the results are very similar to those of L_d. The system is insensitive to errors in R_s. Examples of the stability maps considering parameter errors in R_s at an electrical angular frequency of 200 Hz are shown in Fig. 5.6.

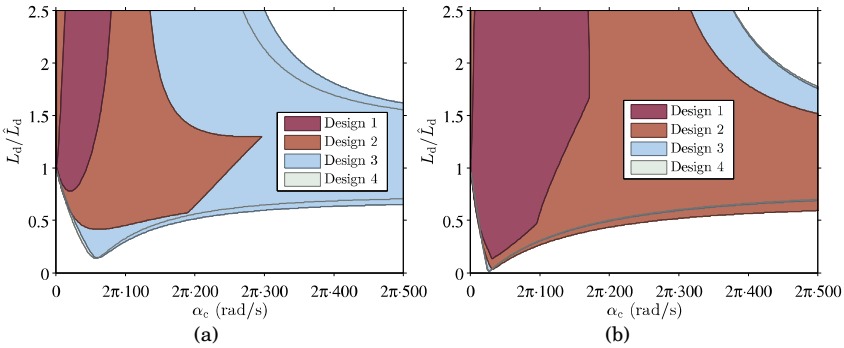

Figure 5.4. Stability maps as a function of the desired bandwidth α_c and the ratio $L_\mathrm{d}/\hat{L}_\mathrm{d}$. The electrical angular frequency is 100 Hz and the sampling frequencies are 1 kHz (a) and 2 kHz (b).

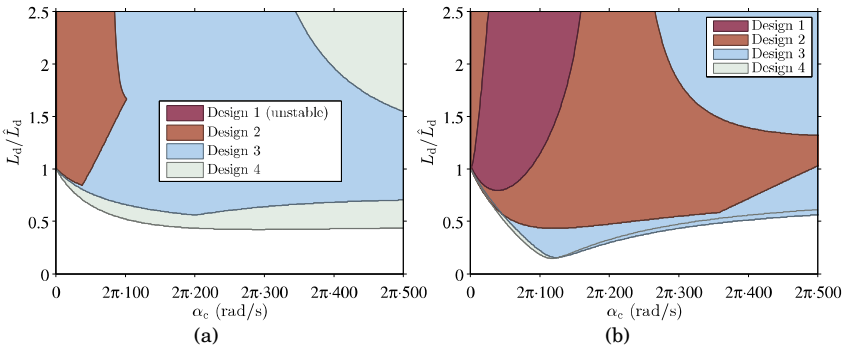

Figure 5.5. Stability maps as a function of the desired bandwidth α_c and the ratio $L_\mathrm{d}/\hat{L}_\mathrm{d}$. The electrical angular frequency is 200 Hz and the sampling frequencies are 1 kHz (a) and 2 kHz (b).

5.2.2 Experimental Results

The discrete-time current controllers were experimentally investigated using a 6.7-kW SyRM drive. Fig. 5.7 shows examples of experimental results at the rotor speed $\omega_\mathrm{m} = 2\pi \cdot 200$ rad/s. The desired bandwidth is $\alpha_\mathrm{c} = 2\pi \cdot 100$ rad/s and the sampling frequency is 2 kHz. Results of the discrete-time design based on the approximate model using the Euler method are shown in Fig. 5.7(a); for comparison, the results of the proposed method are shown in Fig. 5.7(b). The stator voltage is approximately zero until $t = 0.02$ s; however, after the step in $i_\mathrm{d,ref}$, the voltage increases up to about 80% of the rated value. The design based on the Euler approximate model has much noise and leads to some cross-coupling. The performance of the proposed design is much better. The ripple seen in the waveforms originates mainly from the imperfect magnetic saturation model.

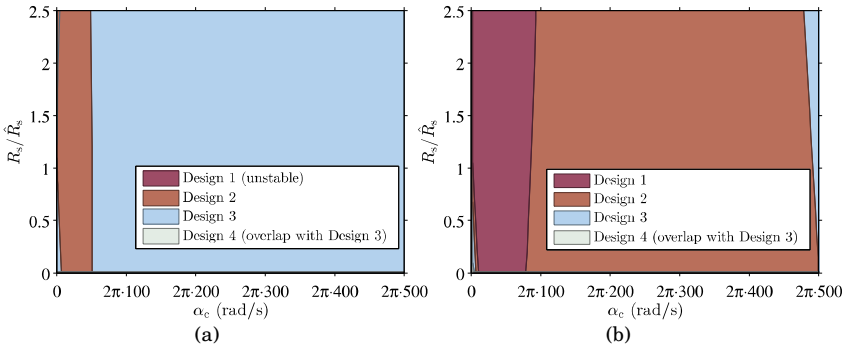

Figure 5.6. Stability maps as a function of the desired bandwidth α_c and the ratio $R_s/\hat{R}_s$. The electrical angular frequency is 200 Hz and the sampling frequencies are 1 kHz (a) and 2 kHz (b).

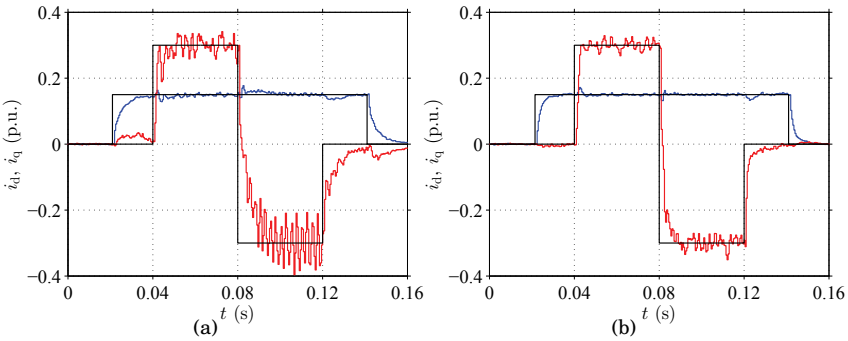

Figure 5.7. Experimental results at a rotor speed of $\omega_m = 2\pi \cdot 200$ rad/s: (a) Discrete-time design based on the approximate model using the Euler method; (b) Discrete-time design based on the exact model. The desired bandwidth is $\alpha_c = 2\pi \cdot 100$ rad/s and the sampling frequency is $f_s = 2$ kHz. Sampled values of i_d (blue), i_q (red), and their references (black) are shown.

6. Summary of Publications

6.1 Abstracts

The abstracts of the publications are reprinted here. Publications I, III and IV deal with loss-minimizing control. Publication II deals with the magnetic saturation model of the SyRM. Publication V considers the flux observer design for sensorless IM drives. Publication VI deals with the discrete current controller design suitable for SyRMs.

Publication I

The paper applies a dynamic space-vector model to loss-minimizing control in induction motor drives. The induction motor model, which takes hysteresis losses and eddy-current losses as well as the magnetic saturation into account, improves the flux estimation and rotor-flux-oriented control. Based on the corresponding steady-state loss function, a method is proposed for solving the loss-minimizing flux reference at each sampling period. A flux controller augmented with a voltage feedback algorithm is applied for improving the dynamic operation and field weakening. Both the steady-state and dynamic performance of the proposed method is investigated using laboratory experiments with a 2.2-kW induction motor drive. The method improves the accuracy of the loss minimization and torque production, it does not require excessive computational resources, and it shows fast convergence to the optimum flux level.

Publication II

This paper deals with the modeling of the magnetic saturation in synchronous reluctance motors (SyRMs). The saturation is modeled by means

of analytical expressions, which can be easily embedded in dynamic equivalent-circuit models. A modified power function—proposed in this paper—can take into account the cross saturation between the orthogonal windings, it is physically consistent, and the number of its parameters is small. The function can be used in real-time control applications and in computer simulations. The model fits well to the experimentally measured inductances of a 6.7-kW SyRM. As an application example, the proposed saturation model was implemented in a full-order observer of a motion-sensorless drive, and experimental results are shown.

Publication III

This paper reviews state-of-the-art loss-minimizing control strategies for synchronous reluctance motors. Methods can be categorized as loss-model controllers (LMCs) and search controllers (SCs). For LMCs, different loss models and the corresponding optimal solutions are summarized. The effects of the core losses and magnetic saturation on the optimal stator current are investigated; magnetic saturation is a more important factor than the core losses. For SCs, different search algorithms are presented and compared. The SCs are evaluated based on their convergence speed, parameter sensitivity, accuracy, and the torque ripple caused by the search process.

Publication IV

This paper proposes a loss-minimizing controller for synchronous reluctance motor drives. The proposed method takes core losses and magnetic saturation effects into account. The core-loss model consists of hysteresis losses and eddy-current losses. Magnetic saturation is modeled using two-dimensional power functions considering cross coupling between the d- and q-axes. The efficiency optimal d-axis current is calculated offline using the loss model and motor parameters. Instead of generating a look-up table, an approximate function was fitted to the loss-minimizing results. The loss-minimizing method is applied in a motion-sensorless drive and the results are validated by measurements.

Publication V

This paper deals with the design of a speed-adaptive full-order observer for sensorless induction motor (IM) drives. A general stabilizing observer

gain matrix, having three free design parameters, is used as a design framework. A gain-scheduled selection of the free design parameters is proposed. Furthermore, the full-order observer is augmented with the stator-resistance adaptation, and the local stability of the augmented observer is analyzed. The performance of the proposed full-order observer design is experimentally compared with a reduced-order observer using a 2.2-kW IM drive.

Publication VI

This paper deals with discrete-time models and current control methods for synchronous motors with a magnetically anisotropic rotor structure, such as interior permanent-magnet synchronous motors (IPMSMs) and synchronous reluctance motors (SyRMs). Dynamic performance of current controllers based on continuous-time models is limited, especially if the ratio of the sampling frequency to the fundamental frequency is low. An exact closed-form hold-equivalent discrete motor model is derived. The zero-order hold of the stator-voltage input is modeled in stationary coordinates, where it physically is. An analytical discrete-time pole-placement design method for a two-degree-of-freedom state-space current controller with an integral action is proposed. The proposed method is easy to apply: only the desired closed-loop bandwidth and the three motor parameters (R_s, L_d, L_q) are required. The robustness of the proposed current control design against parameter errors is analyzed. The controller is experimentally verified using a 6.7-kW SyRM drive.

6.2 Contribution of the Thesis

The main contributions of the thesis can be summarized as follows:

- Loss-minimizing controllers are proposed for IMs and SyRMs which take into account the magnetic saturation effects and core losses. (Publication I, Publication IV)
- A magnetic saturation model is proposed for SyRMs using explicit power functions. (Publication II)
- A gain scheduling method is proposed for a speed-adaptive full-order flux observer for sensorless IM drives. (Publication V)
- An exact discrete-time motor model and discrete-time design of the

current controller suitable for SyRMs are proposed. (Publication VI)

7. Conclusions

This dissertation proposed loss-minimizing control of IM and SyRM drives. Loss-model based methods were used to minimize losses in the motors. The loss-minimizing controllers used motor models that take into account magnetic saturation effects and core losses. The method minimized the loss function for any given torque and speed. The rated flux level usually leads to good energy efficiency at the rated load and speed. However, when the load torque is lower or higher than the rated, the rated flux will not result in maximum efficiency. Speed also affects loss minimization, since core losses depend on the frequency. However, the influence of speed is not as significant as that of torque. The loss-minimizing controllers presented in Publication I and Publication IV adjust the flux (or the d-axis current) based on the torque and speed in order to minimize total losses in the motor. The steady-state energy efficiency has been significantly improved for all the operating points compared to that in the conventional constant-flux approach. The proposed method can slightly increase the energy efficiency compared with those loss-minimizing methods using constant core-loss and inductance parameters.

Based on the parameter sensitivity analysis of the loss-minimizing method, it was found in Publication III that variations in the inductances can affect the optimal flux even more significantly than core-loss model parameters. Furthermore, the saturation model is also very important for the flux observers. These findings motivate the research of developing the magnetic saturation model. The magnetic saturation model of SyRMs was emphatically studied, since the saturation effects in SyRMs are more dramatic. A modified power function model was proposed that takes into account the cross coupling between the orthogonal axes. The proposed saturation model fits well to the measurement results and improves the accuracy of loss minimization and flux estimation.

A drive without a speed or position sensor installed is preferred in many applications. It is well known that sensorless control has instability phenomena in the low-speed region. In order to overcome this problem, a gain scheduling method was proposed for a full-order flux observer in IM drives. The gain design is based on a general stabilizing gain, and the design parameters are selected as functions of speed to guarantee sufficient damping for all operating points, thus improving the robustness, damping and convergence rate of the system. To improve low-speed operation robustness, a resistance-adaptation scheme is applied in the low speed region.

For high-speed applications, where the ratio of the sampling frequency to the fundamental frequency is low, a discrete current controller has been proposed to improve the control stability and performance. A hold-equivalent discrete model was derived for SyRMs, including the effects of the zero-order hold in the stator coordinates. A two-degree-of-freedom state-space current controller with an integral action is applied, and control delay is taken into account in the controller design. Stability analysis, simulations and experiments confirmed that the proposed discrete current controller improves the dynamic performance, robustness, and higher speed or faster current control bandwidth are enabled for limited sampling frequency.

References

F. Abrahamsen, F. Blaabjerg, , J. K. Pedersen, P. Z. Grabowski, and P. Thogersen. On the energy optimized control of standard and high-efficiency induction motors in CT and HVAC applications. *IEEE Trans. Ind. Appl.*, 34(4):822–831, July 1998.

E. Armando, R. Bojoi, P. Guglielmi, G. Pellegrino, and M. Pastorelli. Experimental identification of the magnetic model of synchronous machines. *IEEE Trans. Ind. Appl.*, 49(5):2116–2125, Sept 2013.

A. M. Bazzi and P. T. Krein. Review of methods for real-time loss minimization in induction machines. *IEEE Trans. Ind. Appl.*, 46(6):2319–2328, Nov./Dec. 2010.

F. Blaschke. The principle of field orientation as applied to the new TRANSVEKTOR closed-loop control system for rotating-field machines. *Siemens Rev.*, 34 (5):217–220, 1972.

B. K. Bose and N. R. Patel. A programmable cascaded low-pass filter-based flux synthesis for a stator flux-oriented vector-controlled induction motor drive. *IEEE Trans. Ind. Electron.*, 44(1):140–143, Feb. 1997.

B. Chen, T. Wang, W. Yao, K. Lee, and Z. Lu. Speed convergence rate-based feedback gains design of adaptive full-order observer in sensorless induction motor drives. *IET Electr. Power Appl.*, 8(1):13–22, Jan. 2014.

L. O. Chua. Dynamic nonlinear networks: State-of-the-art. *IEEE Trans. Circuits Syst.*, 27(11):1059–1087, Nov 1980.

K. A. Corzine, B. T. Kuhn, S. D. Sudhoff, and H. J. Hegner. An improved method for incorporating magnetic saturation in the q-d synchronous machine model. *IEEE Trans. Energy Convers.*, 13(3):270–275, Sep. 1998.

H. C. J. de Jong. Saturation in electrical machines. In *Proc. ICEM'80*, volume 3, pages 1545–1552, Athens, Greece, Sep. 1980.

M. Depenbrock. Direct self-control (DSC) of invereter-fed induction machine. *IEEE Trans. Power Electron.*, 3(4):420–429, Oct. 1988.

F. W. Gutzwiller. *GE Silicon Controlled Rectifier Manual*. Liverpool, New York, General Electric Co., 1960.

L. Harnefors. *On analysis, control and estimation of variable-speed drives*. PhD thesis, Dept. Elect. Power Eng., Royal Inst. Tech., Stockholm, Sweden, Oct. 1997.

L. Harnefors. Design and analysis of general rotor-flux-oriented vector control systems. *IEEE Trans. Ind. Electron.*, 48(2):383–390, Apr. 2001.

L. Harnefors and M. Hinkkanen. Complete stability of reduced-order and full-order observers for sensorless IM drives. *IEEE Trans. Ind. Electron.*, 55(3): 1319–1329, Mar. 2008.

L. Harnefors and M. Hinkkanen. Stabilization methods for sensorless induction motor drives: A survey. *IEEE J. Emerging and Sel. Topics in Power Electron.*, 2(2):132–142, June 2014.

L. Harnefors and H.-P. Nee. Model-based current control of AC machines using the internal model control method. *IEEE Trans. Ind. Appl.*, 34(1):133–141, Jan./Feb. 1998.

M. Hinkkanen. Analysis and design of full-order flux observers for sensorless induction motors. *IEEE Trans. Ind. Electron.*, 51(5):1033–1040, Oct. 2004.

M. Hinkkanen and J. Luomi. Modified integrator for voltage model flux estimation of induction motors. *IEEE Trans. Ind. Electron.*, 50(4):818–820, Aug. 2003.

M. Hinkkanen, A.-K. Repo, and J. Luomi. Influence of magnetic saturation on induction motor model selection. In *Proc. ICEM'06*, Chania, Greece, Sept. 2006. CD-ROM.

M. Hinkkanen, L. Harnefors, and J. Luomi. Reduced-order flux observers with stator-resistance adaptation for speed-sensorless induction motor drives. *IEEE Trans. Ind. Electron.*, 25(5):1173–1183, 2010.

K. D. Hurst, T. G. Habetler, G. Griva, and F. Profumo. Zero-speed tacholess IM torque control: simply a matter of stator voltage integration. *IEEE Trans. Ind. Appl.*, 34(4):790–795, July/Aug. 1998.

P. L. Jansen and R. D. Lorenz. A physically insightful approach to the design and accuracy assessment of flux observers for field oriented induction machine drives. *IEEE Trans. Ind. Appl.*, 30(1):101–110, Jan./Feb. 1994.

P. L. Jansen, R. D. Lorenz, and D. W. Novotny. Observer-based direct field orientation: analysis and comparison of alternative methods. *IEEE Trans. Ind. Appl.*, 30(4):945–953, July/Aug. 1994.

A. Kilthau and J. M. Pacas. Appropriate models for the control of the synchronous reluctance machine. In *Conf. Rec. IEEE-IAS Annu. Meeting*, volume 4, pages 2289–2295, Pittsburgh, PA, Oct. 2002.

D. S. Kirschen, D. W. Novotny, and T. A. Lipo. On-line efficieny optimization of a variable frequency induction motor drive. *IEEE Trans. Ind. Appl.*, IA-21(3): 610–616, May/June 1985.

H. Kubota, K. Matsuse, and T. Nakano. DSP-based speed adaptive flux observer of induction motor. *IEEE Trans. Ind. Appl.*, 29(2):344–348, Mar./Apr. 1993.

H. Kubota, I. Sato, Y. Tamura, K. Matsuse, H. Ohta, and Y. Hori. Regenerating-mode low-speed operation of sensorless induction motor drive with adaptive observer. *IEEE Trans. Ind. Appl.*, 38(4):1081–1086, 2002.

C. Mademlis. Compensation of magnetic saturation in maximum torque to current vector controlled synchronous reluctance motor drives. *IEEE Trans. Energy Convers.*, 18(3):379–385, Sep. 2003.

J. A. Melkebeek and J. L. Willems. Reciprocity relations for the mutual inductances between orthogonal axis windings in saturated salient-pole machines. *IEEE Trans. Ind. Appl.*, 26(1):107–114, Jan./Feb. 1990.

J. Millan, P. Godignon, X. Perpina, A. Perez-Tomas, and J. Rebollo. A survey of wide bandgap power semiconductor devices. *IEEE Trans. Power Electron.*, 29 (5):2155–2163, May 2014.

T. Ohtani, N. Takada, and K. Tanaka. Vector control of induction motor without shaft encoder. *IEEE Trans. Ind. Appl.*, 28(1):157–164, Jan./Feb. 1992.

Plexim GmbH. *PLECS User Manual, Version 3.2*. 2012. URL `http://www.plexim.com/files/plecsmanual.pdf`.

S. Sangwongwanich, S. Suwankawin, S. Po-ngam, and S. Koonlaboon. A unified speed estimation design framework for sensorless ac motor drives based on positive-real property. In *Proc. PCC-Nagoya'07*, pages 1111–1118, Nagoya, Japan, Apr. 2007.

P. W. Sauer. Constraints on saturation modeling in AC machines. *IEEE Trans. Energy Convers.*, 7(1):161–167, Mar. 1992.

A. Schönung and H. Stemmler. Static frequency changers with "subharmonic" control in conjunction with reversible variable-speed a.c. drives. *Brown Boveri Rev.*, 51(8/9):555–577, Aug./Sept. 1964.

M.-H. Shin, D.-S. Hyun, S.-B. Cho, and S.-Y. Choe. An improved stator flux estimation for speed sensorless stator flux orientation control of induction motors. *IEEE Trans. Power Electron.*, 15(2):312–318, Mar. 2000.

G. P. Shultz. *Transformers and Motors*. Butterworth-Heinemann, Woburn, MA, 1st edition, 1997.

G. R. Slemon. Modelling of induction machines for electric drives. *IEEE Trans. Ind. Appl.*, 25(6):1126–1131, Nov./Dec. 1989.

I. Takahashi and T. Noguchi. A new quick-response and high-efficiency control strategy of an induction motor. *IEEE Trans. Ind. Appl.*, 22(5):820–827, Sept./Oct. 1986.

P. J. Tsivitse and E. A. Klingshirn. Optimum voltage and frequency for polyphase induction motors operating with variable frequency power supplies. *IEEE Trans. Ind. Gen. Appl.*, 7(4):480–487, July 1971.

A. Vagati, M. Pastorelli, F. Scapino, and G. Franceschini. Impact of cross saturation in synchronous reluctance motors of the transverse-laminated type. *IEEE Trans. Ind. Appl.*, 36(4):1039–1046, Aug. 2000.

G. C. Verghese and S. R. Sanders. Observers for flux estimation in induction machines. *IEEE Trans. Ind. Electron.*, 35(1):85–94, Feb. 1988.

S. N. Vukosavic and E. Levi. Robust DSP-based efficiency optimization of a variable speed induction motor drive. *IEEE Trans. Ind. Electron.*, 50(3):560–570, June 2003.

S. Yamamoto, T. Ara, and K. Matsuse. A method to calculate transient characteristics of synchronous reluctance motors considering iron loss and cross-magnetic saturation. *IEEE Trans. Ind. Appl.*, 43(1):47–56, Jan. 2007.

J.-S. Yim, S.-K. Sul, B.-H. Bae, N. R. Patel, and S. Hiti. Modified current control schemes for high-performance permanent-magnet AC drives with low sampling to operating frequency ratio. *IEEE Trans. Ind. Appl.*, 45(2):763–771, Mar./Apr. 2009.

S. Zhao, O. Wallmark, and M. Leksell. Analysis of a deeply saturated sensorless pmsynrel drive for an automotive application. In *Proc. EPE'11*, pages 1–10, Birmingham, UK, Aug 2011.

Aalto-DD 85/2015

ISBN 978-952-60-6252-5 (printed)
ISBN 978-952-60-6253-2 (pdf)
ISSN-L 1799-4934
ISSN 1799-4934 (printed)
ISSN 1799-4942 (pdf)

Aalto University
School of Electrical Engineering
Department of Electrical Engineering and Automation
www.aalto.fi

BUSINESS +
ECONOMY

ART +
DESIGN +
ARCHITECTURE

SCIENCE +
TECHNOLOGY

CROSSOVER

**DOCTORAL
DISSERTATIONS**